ILASS–Europe 2022, 31th Conference on Liquid Atomization and Spray Systems, 6-8 September 2022, Virtual, Israell

The Influence of Shear-Thinning Behavior on the Impact Morphology of One- and Two-component Drop Film Interactions: A Numerical Investigation

Jonas Steigerwald*[1], Bernhard Weigand[1]
Institute of Aerospace Thermodynamics (ITLR), University of Stuttgart, Germany
*Corresponding author: jonas.steigerwald@itlr.uni-stuttgart.de

Abstract
The impact of a drop onto a liquid film is a highly relevant process which occurs in many technical systems and has been well studied for pure Newtonian liquids. Drop film interactions with non-Newtonian liquids are, however, comparatively seldom investigated, even though such complex fluids are used in many real applications. In this study, we investigate numerically the influence of non-Newtonian (shear-thinning) liquid behavior on the impact morphology of one- and two-component drop film interactions. The simulations are performed with the multiphase flow solver Free Surface 3D (FS3D), which is based on the Volume-of-Fluid (VOF) method and which is capable of simulating shear-thinning liquids as well as multiple miscible liquids. Both frameworks are coupled within this study for the first time which enables simulations of multiple liquids which can exhibit optionally an individual shear-thinning behavior. We investigate the feasibility of an effective viscosity by comparing the impact morphology of interactions involving shear-thinning liquids to morphologies when pure Newtonian liquids are used. Such an approach has the potential to simplify a possible characterization of the impact morphology when shear-thinning liquids are involved. The shear-thinning behavior is modeled by using the Carreau-Yasuda model. An important parameter of this model is the relaxation time λ which represents the reciprocal critical strain rate whose exceedance marks approximately the onset of shear-thinning. We increase λ successively in such a way that the maximum strain rate occurring at the bottom crosses this critical strain rate. This enables a detailed analysis of the onset of the shear thinning behavior during the impact and its influence on the resulting impact morphology.

Keywords
CFD, DNS, Volume-of-Fluid (VOF) method, Drop impact, Non-Newtonian, Shear-thinning, Multi-component liquid

Introduction

The scenario of a drop that impacts onto a thin liquid film is a fundamental process which plays an important role in many technical systems. The resulting impact morphology, whose characterization is of great interest, is highly influenced by many different parameters like the physical properties of the involved liquids [1]. In most studies in literature about drop film interactions Newtonian liquids are used or assumed [1]. However, in many real applications like in ink-jet printing, spray painting or fuel injection in combustion engines the involved liquids can exhibit a non-Newtonian behavior like shear-thinning, viscoelasticity or thixotropy. The influence of rheological properties of such complex liquids on the impact morphology has only been investigated systematically in few studies due to the great experimental and numerical challenges [2-9].

In this study, we investigate numerically the influence of the shear-thinning behavior on the resulting impact morphology of drop film interactions. In general, the modeling of the non-

Newtonian liquid behavior with a viscosity function or with other constitutive equations introduces additional free parameters to the problem of investigation. These parameters enlarge, however, the whole parameter space tremendously, making a full characterization of the impact morphology in consideration of these added parameters almost unfeasible. In order to simplify a potential characterization, it is therefore important to know if the impact outcome of a drop film interaction using non-Newtonian liquids can be reproduced/modeled by using a pure Newtonian liquid with the same effective viscosity. Such an approach is not new as it was already numerically investigated by Focke and Bothe [10] for shear-thinning drop collisions and by Ertl [11] for drop oscillations and jet breakup. In this study, the focus lies on one- and also on two-component drop film interactions, also named unary and binary interactions in the following. The simulations are performed with our in-house multiphase solver Free Surface 3D (FS3D) which is capable of simulating shear-thinning liquids [10,11], multi-component liquids as well as drop film interactions with high accuracy [12-15]. Both numerical frameworks for simulating shear-thinning behavior and multi-component liquids are coupled within this work for the first time. This coupling enables simulations of non-Newtonian multi-component multiphase flows which has to the best of our knowledge never been done before.

Numerical Method

The multiphase flow solver FS3D solves the equations for mass and momentum conservation

$$\partial_t \rho + \nabla \cdot (\rho \mathbf{u}) = 0, \qquad \partial_t (\rho \mathbf{u}) + \nabla \cdot (\rho \mathbf{u} \otimes \mathbf{u}) = \nabla \cdot [\mathbf{S} - \mathbf{I}p] + \rho \mathbf{g} + \mathbf{f}_\gamma + \mathbf{f}_{\nabla\gamma} \qquad \text{(1a,b)}$$

on finite volumes, where $\mathbf{u}$ denotes the velocity vector, ρ the density, $\mathbf{S}$ the incompressible viscous stress tensor, $\mathbf{I}$ the identity matrix, p the pressure and $\mathbf{g}$ the acceleration of gravity. The terms $\mathbf{f}_\gamma$ and $\mathbf{f}_{\nabla\gamma}$ incorporate surface tension and soluto-capillarity at the phase boundary, whereas the latter is only unequal to zero in case different liquids exhibiting different surface tensions interact with each other. The solver uses the Volume-of-Fluid (VOF) method to identify different phases by introducing a scalar field

$$f(\mathbf{x},t) = \begin{cases} 0 & \text{outside the liquid phase,} \\ ]0,1[& \text{in interface cells,} \\ 1 & \text{inside the liquid phase,} \end{cases} \qquad (2)$$

which represents the liquid volume fraction in each control volume [16]. Additional intrinsic averaged VOF variables $\psi_i = V_i/V_l$ can be used optionally to distinguish between different liquids. These variables represent the volume fractions of species i in the liquid volume within a control volume V_l. An ideal and linear mixing behavior without volume expansion is assumed between different species. For the advection of the liquid phase, the transport equations

$$\partial_t f + \nabla \cdot (f u) = 0, \qquad \partial_t (f\psi_i) + \nabla \cdot (f\psi_i u) = 0, \qquad \text{(3a,b)}$$

are solved simultaneously in a closely coupled way with a Strang-splitting approach [17,18]. The corresponding fluxes are calculated geometrically using the piece-wise linear interface calculation (PLIC) method to maintain a sharp interface [19]. The right-hand side of equation (3b) is equal to zero as the problem of investigation is strongly convection-dominated so that molecular diffusion between species can be neglected. The surface tension is modeled by the conservative continuum surface stress (CSS) model by Lafaurie et al. [20].

The conservation equations (1) are solved in a one-field formulation, meaning that all fluids are treated as a single fluid with varying physical properties. These properties φ (e.g. the density ρ) are calculated by

$$\varphi(\mathbf{x},t) = \varphi_g + f(\mathbf{x},t)\left(\varphi_l - \varphi_g\right), \tag{5a-b}$$

where the subscripts g and l denote the gaseous and the liquid phase. In this work, special attention is given to the dynamic viscosity of the liquid μ_l. The different implemented models for its calculation are summarized in the following.

In case of a multi-component liquid flow, the mixture viscosity depends on the individual volume fractions of each species i, so that $\mu_l = \mu_l(\psi_D, \psi_F)$ in the present investigation, where the subscripts D and F denotes the liquids of the drop and film. Several mixture models are implemented in FS3D like for example the mole fraction based models by Bingham [21] and Kendall and Munroe [22] or the volume fraction based binary mixture model by Dey and Biswas [23]. The latter reads

$$\ln \mu_l = \psi_D^2 \ln \mu_D + \psi_F^2 \ln \mu_F + 2\psi_D\psi_F \ln\left(\frac{2\mu_D\mu_F}{\mu_D + \mu_F}\right) \tag{6}$$

and is used throughout this study. The viscous stresses within flowing multi-component liquids could, however, only be modeled with the incompressible Newtonian stress tensor $\mathbf{S} = \mu[\nabla\mathbf{u} + (\nabla\mathbf{u})^{\mathrm{T}}] = 2\mu\mathbf{D}$ with the strain rate tensor $\mathbf{D}$ so far. For simulations with a single one-component liquid, viscous stresses can be calculated either by using the Newtonian stress tensor mentioned above or by using the generalized Newtonian fluid model for purely viscous fluids $\mathbf{S} = 2\mu(\dot{\gamma})\mathbf{D}$, where the viscosity is a function of the shear rate $\dot{\gamma} = \sqrt{2\mathrm{tr}\mathbf{D}^2}$ enabling simulations of shear-thinning and shear-thickening fluids [24]. Several viscosity functions are implemented in FS3D like the two-parameter Ostwald-de Waele power law model $\mu(\dot{\gamma}) = K\dot{\gamma}^{n-1}$, where the material constant K is the flow consistency and the exponent n defines the behavior of the fluid [11,24-26]. Another implemented model that is widely used in literature is the five-parameter Carreau-Yasuda model

$$\mu(\dot{\gamma}) = \mu_\infty + (\mu_0 - \mu_\infty)[1 + (\lambda\dot{\gamma})^a]^{\frac{n-1}{a}}, \tag{7}$$

where μ_0 and μ_∞ denote the zero- and infinite-shear-rate viscosities, a is a material constant and λ denotes the characteristic relaxation time which marks roughly the transition between the Newtonian and the non-Newtonian behavior [11,27-29].

Even though a numerical interconnection of both multi-component and non-Newtonian frameworks is relatively straight forward, difficulties arise when two different liquids begin to mix. The reason for this is that a viscosity function for μ_l is needed where the viscosity is a function of ψ_i, $\dot{\gamma}$ and other parameters like the exponent n. Since such an equation is not known to the authors, a generic model was constructed based on simple underlying assumptions to enable non-Newtonian multi-component multiphase flow simulations.

A simple generic shear-rate dependent viscosity function for binary liquid mixtures

The basis of the constructed viscosity function is the Carreau-Yasuda model (equation (7)), whose five parameters $(\mu_0, \mu_\infty, a, \lambda, n)$ are now functions of the species volume fractions ψ_i. The model reads

$$\mu_l(\dot{\gamma}, \tilde{\mu}_0, \tilde{\mu}_\infty, \upsilon_a, \upsilon_\lambda, \upsilon_n) = \tilde{\mu}_\infty + (\tilde{\mu}_0 - \tilde{\mu}_\infty)[1 + (\upsilon_\lambda\dot{\gamma})^{\upsilon_a}]^{\frac{\upsilon_n - 1}{\upsilon_a}}, \tag{8a}$$

with

$$\tilde{\mu}_\eta = \tilde{\mu}_\eta(\psi_1, \psi_2) = {\mu_{1,\eta}}^{\psi_1^2} {\mu_{2,\eta}}^{\psi_2^2} \left(\frac{2\mu_{1,\eta}\mu_{2,\eta}}{\mu_{1,\eta} + \mu_{2,\eta}}\right)^{2\psi_1\psi_2}, \tag{8b}$$

$$\upsilon_\eta(\psi_1,\psi_2)=\begin{cases}\eta_1 & \text{if only liquid 1 is shear-thinning,}\\ \eta_2 & \text{if only liquid 2 is shear-thinning,}\\ \eta_1\psi_1+\psi_2\eta_2 & \text{if both liquids are shear-thinning.}\end{cases} \tag{8c}$$

For a zero and infinite shear rate or for the viscosity limits, respectively, it is assumed that a viscosity mixture model (equation (6)) can be used to calculate the viscosity limits for a specific mixture composition (equation (8b)). Note that $\mu_{i,0}=\mu_{i,\infty}$ in case liquid i shows pure Newtonian behavior. Furthermore, an assumption has to be made about the other parameters of this shear-thinning model for a specific mixture composition. We assume that the parameters remain the same but in case both liquids exhibit non-Newtonian behavior the resulting parameters are calculated as a weighted mean (see equation (8c)). At this point it should be mentioned that the actual definition of $\upsilon_\eta(\psi_1,\psi_2)$ (equation (8c)) had an insignificant effect on the resulting morphologies of the simulated impact scenarios. The reasons for this are that both liquids hardly mix during the interaction and that only a tiny fraction of control volumes with $f>0$ contain both species due to the high spatial resolution.

Validation

The numerical coupling between non-Newtonian viscosity treatment and the multi-component framework is validated against a derived analytical solution of a steady laminar three-layered plane Poiseuille flow with two different Ostwald-de Waele power law fluids (Layer A and B) and one Newtonian fluid (Layer C). The solution was derived following the approach of Bird [30] and Xenakis [31] and reads

$$u(y)=\begin{cases}-\dfrac{F_x(y^2-L^2)}{2\mu_C}+c_1\dfrac{(y-L)}{\mu_C} & \text{if } \beta\le y\le L, \quad \text{(Layer C)}\\ G(B,y,\beta)-\dfrac{F_x(\beta^2-L^2)}{2\mu_C}+c_1\dfrac{(\beta-L)}{\mu_C} & \text{if } \alpha\le y<\beta, \quad \text{(Layer B)}\\ G(A,y,0) & \text{if } 0\le y<\alpha, \quad \text{(Layer A)}\end{cases} \tag{9a-c}$$

with

$$G(i,\xi,\zeta)=-\left(\frac{1}{\mu_i}\right)^{n_i^{-1}}\left(\frac{n_i}{n_i+1}\right)\frac{(-F_x\xi+c_1)^{n_i^{-1}+1}-(-F_x\zeta+c_1)^{n_i^{-1}+1}}{F_x}, \tag{9d}$$

where F_x denotes the flow driving body force, L the channel height, α and β the interface positions between the layers, and μ_i and n_i denote the dynamic viscosity and the power-law exponent of layer i. The unknown constant c_1 is determined numerically with equation $G(A,\alpha,0)=G(B,\alpha,\beta)+u_C(\beta)$ by means of the Newton-Raphson method.

Two different scenarios were simulated, in which $\mu_C=1\,\mathrm{mPa\,s}$ and the fluid of layer A is treated as a shear-thinning fluid with $n_A=0.6$ and $\mu_A=20\,\mathrm{mPa\,s}$ ($K_A=20\,\mathrm{mPa\,s^{0.6}}$) in both cases. In the first case, the fluid in layer B is treated as a Newtonian fluid ($\mu_B=4\,\mathrm{mPa\,s}$), whereas in the second case the fluid exhibit shear-thickening behavior with $n_B=1.8$ ($K_B=4\,\mathrm{mPa\,s^{1.8}}$). The other parameters are set to $L=1\,\mathrm{m}$, $\alpha=0.375\,L$, $\beta=0.625\,L$, $F_x=0.1\,\mathrm{N/m^3}$. The resulting velocity profiles for $N_y=32$ grid cells per channel height L are depicted in figure 1a, where the velocity is made non-dimensional by using the resulting averaged velocity $\bar{u}$. As can be seen, the simulated velocity profiles almost coincide with the analytical solution which validates the numerical implementations. Figure 1b shows the mean relative error ε for four different grid resolutions. Even for a very coarse grid resolution with $N_y=16$ the error ε is less than 2%. The results converge with first order due to the fact, that for the calculation of $\dot{\gamma}$ some needed face velocities are calculated as arithmetic means. All velocity gradients are, however, calculated by means of central differences.

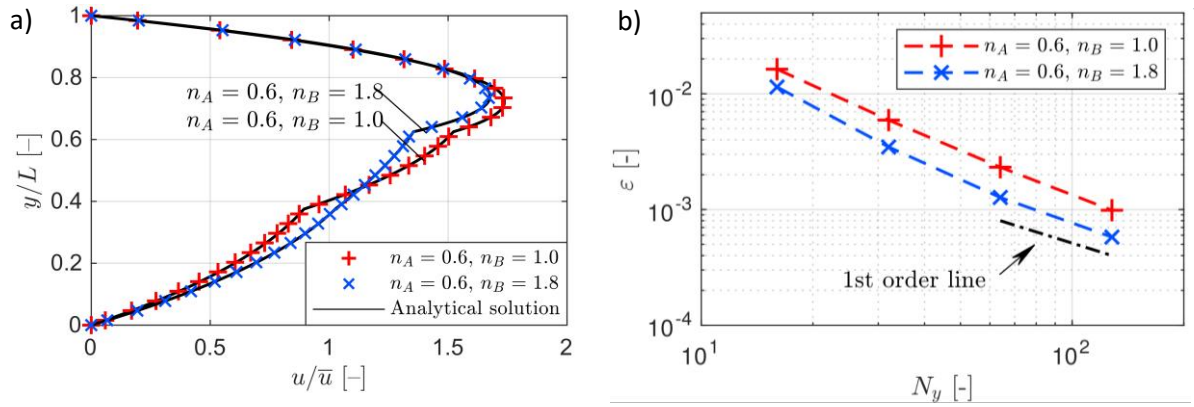

Figure 1. (a) Comparison between the numerical result for $N_y = 32$ and the analytical solution and (b) the evaluated mean relative error $\varepsilon = N_y^{-1} \sum_j |u_{j,\mathrm{num}} - u_{j,\mathrm{ana}}| / u_{j,\mathrm{ana}}$ for several grid resolutions.

Setup

The computational setup is almost identical to the one used by Steigerwald et al. [12-13] and is, therefore, only shortly described. A spherical drop with diameter $D = 2.5\ \mathrm{mm}$ is initialized in a distance of $2D$ above a liquid film of thickness $h = 0.5\ \mathrm{mm}$ within a cubic domain with dimension $(7D)^3$. As the impact scenario is fully symmetrical, only a quarter of the drop film interactions are simulated. The drop exhibits an initial velocity $U = 3.4\ \mathrm{m/s}$ towards the film. The computational domain is discretized with a Cartesian grid consisting of 512³ cells, whereas the impact region with dimensions $(1.5D)^3$ is discretized equidistantly with 256³ cells. This grid resolution is sufficient to accurately reproduce numerically the impact morphology [12]. Outside the impact region a stretched cell arrangement is used. A no-slip boundary condition is applied at the bottom and besides the two symmetry boundary conditions homogeneous Neumann boundary conditions are applied at all remaining sides.

In this study, the liquid density is set to $\rho = 900\ \mathrm{kg/m^3}$ for both liquids and the surface tension is set to $\sigma = 73.15\mathrm{N/m}$ which results in an impact Weber number $We = \rho D U^2/\sigma = 356$. Furthermore, four of the five parameters of the Carreau-Yasuda model remain the same throughout this study. These are the zero- and infinite-shear-rate viscosities $\mu_0 = 0.050\ \mathrm{Pas}$ and $\mu_\infty = 0.005\ \mathrm{Pas}$, the exponent $n = 0.6$ and the material constant $a = 1.5$. This leads to a minimum and maximum Reynolds number of $Re_0 = 153$ and $Re_\infty = 1530$. Thus, all simulated impact scenarios lie in the deposition regime with a maximum splashing parameter of $\bar{K} = We^{0.5} Re_\infty^{0.25} / (2164 + 7560\delta^{1.78})^{0.625} = 0.87$ with a dimensionless film thickness $\delta = h/D = 0.2$ [32-33]. The physical properties of the surrounding medium are set to those of ambient air. The parameter that is varied within this study is the relaxation time λ, which roughly marks the transition from the Newtonian (N) to the non-Newtonian (nN)/shear-thinning regime. The various λ are chosen in a way that $\bar{\mu} \in \{0.125, 0.25, 0.5, 0.75, 0.9\}$ with

$$\bar{\mu} = (\mu - \mu_\infty)/(\mu_0 - \mu_\infty) = \left(1 + \left(\lambda \dot{\gamma}_{max,N0-N0}\right)^a\right)^{(n-1)/a}, \tag{10}$$

where $\dot{\gamma}_{max,N0-N0} = \dot{\gamma}_R = 18060\mathrm{s}^{-1}$ denotes the maximum occurring shear rate at the bottom during the unary N-N interaction with μ_0. The resulting viscosity functions are visualized in figure 2. The vertical dashed-dotted lines show the corresponding critical shear rates $\dot{\gamma}_{cr} = \lambda^{-1}$. For the unary non-Newtonian interactions (nN-nN), both drop and film liquid exhibit a shear-thinning behavior, whereas for the binary N-nN interactions the drop viscosity is $\mu_D = \mu_0$ and only the film liquid exhibit a shear-thinning behavior.

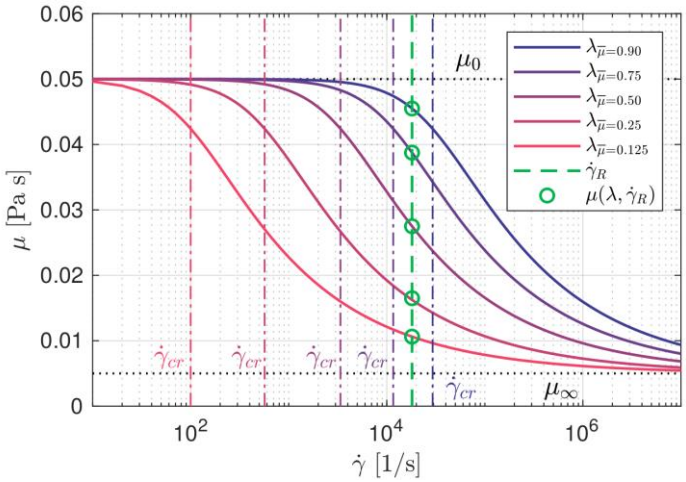

Figure 2. Viscosity functions $\mu(\dot{\gamma})$ obtained with the Carreau-Yasuda model with $\mu_0 = 0.050$ Pas, $\mu_\infty = 0.005$ Pas, $n = 0.6$, $a = 1.5$ for $\lambda_{\overline{\mu}=0.90}$, $\lambda_{\overline{\mu}=0.75}$, $\lambda_{\overline{\mu}=0.50}$, $\lambda_{\overline{\mu}=0.25}$ and $\lambda_{\overline{\mu}=0.125}$ together with the critical shear rates $\dot{\gamma}_{cr} = \lambda^{-1}$.

Results

Figure 3 shows the side view of the impact morphology with the instantaneous viscosity field $\overline{\mu}(\mathbf{x}, t)$ of two unary nN-nN interactions for two different times $\overline{t} = tU/D = 0.5$ and $\overline{t} = 2.5$. For $\lambda_{\overline{\mu}=0.50}$ (figure 3a), the local shear rates within the liquid are already high enough so that the viscosity $\overline{\mu}$ decreases due to shear-thinning. The lowest viscosity values are reached during the early stages of the impact $\overline{t} < 0.5$ at the bottom, where the maximum shear stress occurs at the foot of the crown where the liquid is strongly deflected. At later times, the local shear rates decrease and so the influence of shear-thinning. For $\lambda_{\overline{\mu}=0.125}$ (figure 3b), the local viscosity within the crown is already close to the infinite-shear-rate viscosity at $\overline{t} = 0.5$ and remains low also at later times. A comparison with the interaction with $\lambda_{\overline{\mu}=0.50}$ shows that shear-thinning effects can indeed affect the shape of the crown. Besides that, the evaluation of all performed simulations shows that the maximum occurring shear rate at the bottom during the interaction $\dot{\gamma}_{max}$ can serve as a reasonable reference point to estimate the onset of shear-thinning influence in these interactions with $\lambda = \dot{\gamma}_{max}{}^{-1}$.

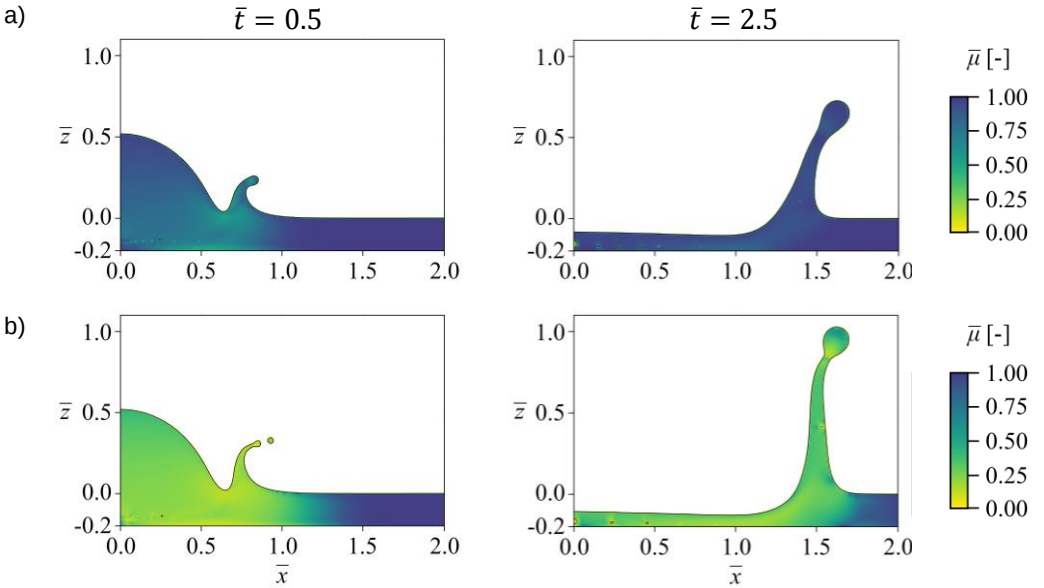

Figure 3. Side views of the impact morphology of unary nN-nN interactions with instantaneous viscosity distribution $\bar{\mu}(\mathbf{x}, t)$ inside the liquid phase at $\bar{t} = 0.5$ and $\bar{t} = 2.5$ for a) $\lambda_{\overline{\mu}=0.50}$ and b) $\lambda_{\overline{\mu}=0.125}$.

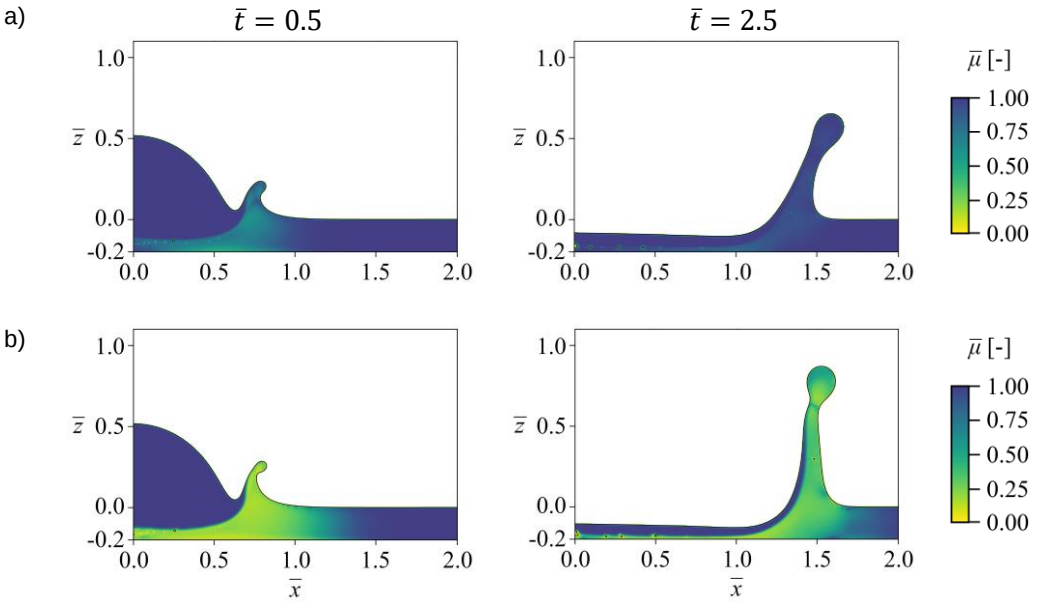

Figure 4. Side views of the impact morphology of binary nN-nN interactions with instantaneous viscosity distribution $\bar{\mu}(\mathbf{x}, t)$ inside the liquid phase at $\bar{t} = 0.5$ and $\bar{t} = 2.5$ for a) $\lambda_{\overline{\mu}=0.50}$ and b) $\lambda_{\overline{\mu}=0.125}$.

Figure 4 shows again side views of the impact morphology with the internal $\overline{\mu}$ field but of binary N-nN interactions. The qualitative observations are identical to the unary case. In both unary and binary interactions the apparent viscosity of the film liquid are nearly the same for the individual λ. However, the crown growth is reduced by the high and constant viscosity of the Newtonian drop liquid, as can be seen by comparing figure 4b with figure 3b.

In the following, we evaluate the effective viscosity of all simulated interactions by comparing the resulting maximum non-dimensional crown heights $\overline{H}_{CR,max} = H_{CR,max}/D$ with the resulting heights of Newtonian reference cases. For an accurate mapping, we first fit $\overline{H}_{CR,max}$ of the Newtonian cases as a function of $\bar{\mu} = (\mu - \mu_\infty)/(\mu_0 - \mu_\infty)$ with $0 \leq \bar{\mu} \leq 1$ (see figure 5a). Next, these cubic fitting equations are used to evaluate the effective viscosities $\bar{\mu}_{eff}$ of the unary nN-nN and binary N-nN interactions. The resulting $\bar{\mu}_{eff}$ are plotted in figure 5b over the Carreau number $Cu = \lambda U/D$. Note that the definition of the Carreau number is identical to the one of the Deborah number $De = \lambda U/D$, which is widely used in studies involving complex liquids and which is used to estimate the influence of an elastic behavior of the fluid on the flow. As we only investigate shear-thinning behavior and an elastic behavior is not modeled in this work, we stay with Cu in order to prevent misunderstandings. Firstly, it is interesting to observe that the obtained distributions $\overline{\mu}_{eff}(Cu)$, shown in figure 5b, are very similar for both unary and binary interactions. Besides that, both distributions exhibit a great similarity with the viscosity functions used for the simulations (see figure 2). Motivated by this similarity, we fitted both distributions with functions exhibiting the same structure as the used Carreau-Yasuda model which thus read

$$\bar{\mu}_{eff} = (1 + (C_1 Cu)^{C_2})^{(C_3-1)/C_2}, \tag{11}$$

where C_1, C_2, and C_3 are constants. For the unary nN-nN interactions we obtain $C_1 = 9.36$, $C_2 = 1.67, C_3 = 0.67$ and $C_1 = 6.76, C_2 = 1.65, C_3 = 0.6$ for the binary N-nN interactions. The small relative errors $\epsilon = 0.41\%$ and $\epsilon = 0.65\%$ for the unary and binary interactions confirm that both distributions can be fitted very well with equation (11). Both fitting equations are plotted in figure 5b. Furthermore, it is worth mentioning that the constants C_2 and C_3 are very

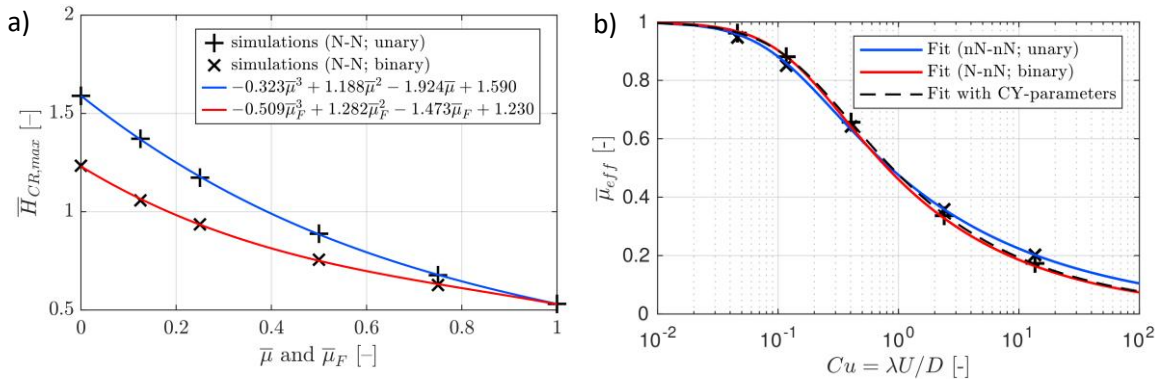

Figure 5. (a) $\overline{H}_{CR,max}$ plotted over $\bar{\mu}$ for both unary and binary N-N interactions together with cubic fitting equations. The subscript F denotes that in the binary interactions only the viscosity of the film liquid is varied; (b) Effective viscosity $\overline{\mu}_{eff}(Cu)$ together with the fitting equation (X) and the belonging constants $C_1 = 9.36, C_2 = 1.67, C_3 = 0.67$ (nN-nN; unary), $C_1 = 6.76$, $C_2 = 1.65, C_3 = 0.6$ (N-nN; binary) and $C_1 = 6.08, C_2 = a = 1.5, C_3 = n = 0.6$ using the set parameters of the Carreau-Yasuda model.

similar to the constants of the used viscosity function with $a = 1.5$ and $n = 0.6$, especially for the binary N-nN interactions. A fitting equation (11) with $C_1 = 6.08$, $C_2 = a = 1.5$ and $C_3 = n = 0.6$ with $\epsilon = 2.25\%$ regarding both distributions is also plotted with a dashed line in figure 5b. The good agreement between the numerical results and this fitted equation, which has the same parameters as the used viscosity function in the simulations raises an important question: Can the proposed fitting equation (11) also be used to fit numerical results in case other Carreau-Yasuda model parameters a and n are used with $C_2 = a$ and $C_3 = n$ and is C_1 therefore the only constant that has to be determined? If this is the case, this will greatly simplify the characterization of the impact morphology of both unary and binary interactions involving shear-thinning liquids.

Conclusion

A numerical study about the influence of a shear-thinning liquid behavior on the impact morphology in drop film interactions was presented. The study encompassed not only one- but also the first ever simulated two-component drop film interactions involving shear-thinning liquids. In order to enable non-Newtonian multi-component multiphase flow simulations, we used the in-house solver FS3D whose previous capabilities of simulating multiple distinguishable liquids and shear-thinning liquids were coupled. The new interconnection between both frameworks was validated by a comparison with an analytical solution of a three-layered plane Poiseuille flow.

Starting point of the presented parameter study was an impact scenario in the deposition regime. In several simulations, the relaxation time λ, a parameter of the used Carreau-Yasuda model, was varied. It was shown that the maximum occurring shear rate at the wall can be used to estimate the onset of the influence of a shear-thinning behavior with $\dot{\gamma}_{max}^{-1} = \lambda_{cr}$ and that a shear-thinning behavior can indeed influence the morphology of the resulting crown. In a next step, the concept of an effective viscosity has been tested with regard to a potential simplification of the morphology characterization when shear-thinning liquids are involved in drop film interactions. The concept was analyzed by using the maximum occurring crown height $\overline{H}_{CR,max}$. The obtained distributions $\overline{\mu}(Cu = \lambda U/D)$ exhibit a great similarity with the used viscosity function $\overline{\mu}(\dot{\gamma})$ for both unary and binary interactions and both distributions $\overline{\mu}(Cu)$ could be fit very well with a function almost identical to the used Carreau-Yasuda model. This result raises the question if the impact morphology of both one- and two-component drop film

interactions involving shear-thinning liquids can be predicted in general if an accurate description of the shear-thinning behavior of the used liquid and the corresponding fits of the Newtonian reference cases are known. If this is the case, this will greatly simplify the overall description of the impact morphology of such interactions. However, this hypothesis has to be investigated in future studies.

Acknowledgements

The authors kindly acknowledge the financial support of the Deutsche Forschungs-gemeinschaft (DFG) through the projects SFB-TRR75 (84292822) and EXC 2075 (390740016). In addition, the authors kindly acknowledge the High Performance Computing Center Stuttgart (HLRS) for support and supply of computational time on the HPE Apollo system “Hawk” under Grant No. FS3D/11142.

References

[1] Liang, G and Mudawar, I., 2016, Int J Heat Mass Tran, 101, pp. 577-599.
[2] Lampe, J., DiLalla, R., Grimaldi, J., and Rothstein, J. P., 2005, J Nonnewton Fluid Mech, 125 (1), pp. 11–23.
[3] Blackwell, B. C., Deetjen, M. E., Gaudio, J. E., and Ewoldt, R. H., 2015, Phys. Fluids, 27 (4), p. 043101.
[4] Sen, S., Morales, A. G., and Ewoldt, R. H., 2020, J. Fluid Mech., 2020, 891, A27.
[5] Sen, S., Morales, A. G., and Ewoldt, R. H., 2021, Phys. Rev. Fluids, 6 (4), p. 043301.
[6] Mohammad Karim, A., 2020, Phys. Fluids, 32 (4), p. 043102.
[7] López-Herrera, J., Popinet, S., and Castrejón-Pita, A., 2019, J Nonnewton Fluid Mech, 264, pp. 144–158.
[8] Rezaie, M. R., Norouzi, M., Kayhani, M. H., and Taghavi, S. M., 2021, Meccanica, 56 (8), pp. 2021–2038.
[9] Peng, X. (彭小芸), Wang, T. (王天友), Sun, K. (孙凯) and Che, Z. (车志钊), 2021, Phys. Fluids, 33, 112106.
[10] Focke, C. and Bothe, D., 2011, J Nonnewton Fluid Mech, 166 (14), pp. 799-810.
[11] Ertl, M., 2019, Ph.D. thesis, University of Stuttgart, Germany.
[12] Steigerwald, J., Ibach, M., Reutzsch, J. and Weigand, B., 2021, Chapt. 17 in: “High Performance Computing in Science and Engineering ’20”, Springer.
[13] Steigerwald, J., Geppert, A. and Weigand, B., 29 Aug. - 2 Sept. 2021, 15th Triennial International Conference on Liquid Atomization and Spray Systems, Edinburgh, UK.
[14] Rieber, M., Frohn, A., 1999, Int. J Heat Fluid Flow, 20 (5), pp. 455–461.
[15] Fest-Santini, S., Steigerwald, J., Santini, M., Cossali, G.E. and Weigand, B., 2021, Comput. Fluids, 214, 104761.
[16] Hirt, C. W. and Nichols, B. D., 1981, J Comput Phys, 39 (1), pp. 201-225.
[17] Strang, G., 1968, SIAM J. Numer. Anal. 5, pp. 506–517.
[18] Weymouth, G. D. and Yue, D. K.-P., 2010, J Comput Phys, 229(8), pp. 2853-2865.
[19] Rider, W. J. and Kothe, D. B., 1998, J Comput Phys, 141(2), pp. 112-152.
[20] Lafaurie, B., Nardone, C., Scardovelli, R., Zaleski, S., and Zanetti, G., 1994, J Comput Phys, 113 (1), pp. 137-147.
[21] Bingham, E. C., 1922, "Fluidity and plasticity", Mcgraw - Hill, New York.
[22] Kendall, J. and Munroe K. P., 1917, J. Am. Chem. Soe., 38, pp. 1787–1802.
[23] Dey, R. and Biswas, P., 2018, J Mol Liq, 265 (1), pp. 356-360.
[24] Irgens, F., 2014, “Rheology and Non-Newtonian Fluids”, Springer Cham.
[25] Ostwald, W., 1925, Kolloid-Zeitschrift 36, pp. 99-117.
[26] De Waele, A., 1923, Oil Color Chem. Assoc. J. 6, pp. 33-88.
[27] Bird, R. B., Armstrong, R. C., Hassager, O., 1987, “Dynamics of Polymeric Liquids. Vol. 1, 2nd Ed.: Fluid Mechanics”, Wiley.
[28] Carreau, P. J., 1968, Ph.D. thesis, University of Wisconsin, Madison, USA.
[29] Yasuda, K., 1979, Ph.D. thesis, Massachusetts Institute of Technology, Cambridge, USA
[30] Bird, R. B., Stewart, W. E., Lightfoot, E. N., 2002, “Transport Phenomena 2nd Ed.”, Wiley.
[31] Xenakis, A., 2015, Ph.D. thesis, University of Manchester, UK.
[32] Marengo, M. and Tropea, C., 1999, DFG, Tr 194/10 1,2.
[33] Geppert, A., Chatzianagnostou, D., Meister, C., Gomaa, H., Lamanna, G., and Weigand, B., 2016, Atomization Sprays, 26 (10), pp. 983–1007.